 CMC, vol.19, no.2, pp.105-133, 2010

Ionic Polymer Metal Composite Flapping Actuator Mimicking Dragonflies

Sujoy Mukherjee[1] **and Ranjan Ganguli**[1,2]

Abstract: In this study, variational principle is used for dynamic modeling of an Ionic Polymer Metal Composite (IPMC) flapping wing. The IPMC is an Electroactive Polymer (EAP) which is emerging as a useful smart material for 'artificial muscle' applications. Dynamic characteristics of IPMC flapping wings having the same size as the actual wings of three different dragonfly species *Aeshna Multicolor*, *Anax Parthenope Julius* and *Sympetrum Frequens* are analyzed using numerical simulations. An unsteady aerodynamic model is used to obtain the aerodynamic forces. A comparative study of the performances of three IPMC flapping wings is conducted. Among the three species, it is found that thrust force produced by the IPMC flapping wing of the same size as *Anax Parthenope Julius* wing is maximum. Lift force produced by the IPMC wing of the same size as *Sympetrum Frequens* wing is maximum and the wing is suitable for low speed flight. The numerical results in this paper show that dragonfly inspired IPMC flapping wings are a viable contender for insect scale flapping wing micro air vehicles.

Keywords: Ionic polymer metal composite, dynamics, actuator, flapping, smart materials, unsteady aerodynamics, micro air vehicles.

Nomenclature

A	Generalized coordinate of mechanical displacements
b	Width of IPMC flapping wing
c	Airfoil chord
C_n	Normal force coefficient

[1] Department of Aerospace Engineering, Indian Institute of Science, Bangalore – 560012, India.
[2] Corresponding author,ganguli@aero.iisc.ernet.in.

$\mathbf{c}^D$	Stiffness matrix at constant electric displacement
$(C_d)_f$	Drag coefficient due to skin friction
$\mathbf{C}^{-1}$	Inverse of capacitance
d	Strain coefficient
D	Electric displacement vector
f	Force vector
h_t	Thickness of IPMC flapping wing
$\mathbf{h}$	Electromechanical coupling matrix
j	Square root of -1
$\mathbf{K}_s$	Diagonal stiffness matrix
L_f	Unsupported length of IPMC flapping wing
L_t	Total length of IPMC flapping wing
L_u	Differential operator
$\mathbf{M}_s$	Diagonal mass matrix
q	Generalized coordinate of electric displacements
s	Laplace variables
T	Stress vector
T	Kinetic energy
U	Flight speed
v	Electric potential applied on each electrode

V	Relative velocity
V_x	Flow speed tangential to the section
V	Potential energy
V_{se}	Strain energy
V_{couple}	Coupling potential energy
$V_{dielectric}$	Dielectric potential energy
w	Deflection in X_3 direction
W^{ext}	Work done by external force
X_i	Cartesian axes (i=1,2,3)
y	Coordinate along the semispan
α_0	Angle of section's zero lift line
α'	The flows relative angle of attack at the $3/3$ chord location
β_n	Eigenvalues
δ	Variation
ε^T	Dielectric permittivity matrix at constant stress
η_s	Leading edge suction efficiency
θ	Pitch angle of chord with respect to U
$\bar{\theta}_a$	Pitch angle of flapping axis with respect to U
$\bar{\theta}_w$	Mean pitch angle of chord with respect to flapping axis
ρ	Density of IPMCs

ρ_{air}	Atmospheric density
σ_n	Constant
υ_2	Mid-chord normal velocity component due to the wing's motion
Φ_f	Flapping angle
Φ_u	Mechanical shape functions
Φ_D	Electrical shape functions
Ψ	Coupling vector
ω	Frequency
$(\ )_{,xx}$	Second derivative with respect to space

1 Introduction

In recent years, Micro Air Vehicles (MAVs) have attracted a great deal of attention which is driven by applications ranging from civil search-and-rescue missions to military surveillance missions. In order to perform these tasks, MAVs are required to fly slowly, maneuver with great precision and navigate through complex environments. Nature provides flapping flyers such as birds and insects which routinely exhibit such performance [Ganguli et al. (2010)]. These natural flapping flyers represent a very successful design for intelligent MAVs with much better performance than conventional wings and rotors [Ansari et al. (2006)]. Hence, birds and insects serve as a natural source of inspiration for the development of MAVs. For a flapping-wing MAV, the wings are not only responsible for lift, but also for propulsion and maneuvers. Therefore, MAV flapping wing design represents one of the major challenges to efficient flight in the low Reynolds-number regime [Singh and Chopra (2008), Yamada and Yoshimura (2008)].

In order to mimic the wing movement of the natural flapping flyers, such as birds and insects, several researchers have developed biomimetic flapping wing mechanisms. These mechanisms are used to achieve a deeper insight as well as qualitative and quantitative comprehension of flapping flight. Several biomimetic flapping wing mechanisms were developed to mimic the wing motion of birds such

as humming birds [Raney and Slominski (2004), McIntosh et al. (2006)]. On the other hand, several researchers developed biomimetic flapping wing mechanisms to mimic the wing motion of insects such as hawkmoth [VandenBerg and Ellington (1997)], fruit fly [Dickinson et al. (1999)], dragonfly [Yamamoto and Isogai (2005)] etc. Insects, such as dragonfly, are very efficient flyers and its flight satisfies the entire flight envelope required for an MAV. Dragonflies are one of only a few species of insects that are capable of gliding flight. Moreover, dragonflies are among the largest of the flying insects and have a relatively small wing stroke angle. Therefore, dragonfly characteristics can provide design guidelines for the development of flapping wing MAVs. Flight mechanics of different dragonfly species have been studied extensively by many researchers. Zhang and Lu (2009) used a multiblock lattice Boltzmann method to study the aerodynamic performance due to forewing and hindwing interaction in gliding flight of dragonfly *Sympetrum sanguineum*. Wang et al. (2002) measured the body position, attitude and wing deformation of a free-flight dragonfly *Ploycanthagyna melanictera*. In another study, Kesel et al. (1998) analyzed the mechanical load-bearing capacity of a dragonfly *Aeshna cynea* wing. It can be noted from the above studies that biomimetic flapping wing mechanisms have very important contributions in the fundamental understanding of the flapping flight. However, these dynamically scaled flapping wing mechanisms may not be suitable for use in small or micro-scale flying vehicles as they are bulky and flap at very low frequency. Moreover, current flapping wing mechanisms rely on pneumatic and motor-driven flapping actuators which lead to high weight and system-complexity [Park et al. (2005)]. Natural flapping flyers generate lift and thrust using complex wingbeat kinematics which cannot be easily mimicked with these conventional actuators. Another plausible alternative may be to use actuators made of smart materials.

The field of smart materials has seen enormous research growth in the past two decades [Cheng and Chen (2004), Wu et al. (2005)]. Smart materials, such as piezoelectric materials [Zhang (2004), Sladek et al. (2006), Apte and Ganguli (2009)], shape memory alloys [Auricchio et al. (2003), Kanca and Eskil (2009)], magnetostrictive materials [Ghosh and Gopalakrishnan (2004), Zhou et al. (2007)] etc., are being considered for various applications. Several researchers have suggested piezoceramics for actuating the motion of flapping wings [Cox et al. (2002)]. However, such concepts suffer from high weight penalty, high voltage demand and low actuation authority problems. Ionic polymer metal composites (IPMCs) are ionic Electroactive Polymers (EAP), which is an emerging class of smart materials. IPMCs consist of a thin polyelectrolyte membrane and a type of noble metal, such as gold and platinum, chemically plated on both sides of the membrane. An IPMC can undergo a fast and large bending motion when a low electric potential

is applied to its electrodes. When the electric field is applied, the cations are moving toward cathode dragging molecules of solvents. This motion causes volume increase in the cathode side and volume reduction in the opposite side. The total motion of the ions and molecules of the solvent creates bending motion which provides the source of actuation force of the IPMCs. The similarity in behavior of these materials to biological muscles acquired them the moniker "artificial muscles" [Bar-Cohen (2004)]. Interesting properties, such as softness, lightness (1-2.5 g cm^{-3}), fast reaction speed (μs to s), large bending displacement (>10%), and low activation voltage (1-7 volt), make IPMCs promising candidates for the design of a flapping wing [Shahinpoor et al. (1998)]. Park et al. [Park et al. (2005)] designed a flapping wing actuated by IPMC but they used static modeling method for the simulation of the wing. Lee et al. (2006) improved the performance of the IPMC flapping actuator in terms of solvent loss characteristics and actuation force. They transferred the bending motion created by IPMC to a flapping motion through a rack and pinion system. However, their experimental investigation indicates that the actuator is useful at low frequency.

Researchers have made IPMCs more attractive for dynamic actuation in the past few years. Bennett et al. (2006) showed that the use of ionic liquid rather than water as a solvent in IPMC is advantageous because it removes the hydration dependence. Akle et al. (2006) proposed a novel manufacturing method using ionic liquid to produce high strain air-stable IPMC structure which can sustain higher voltage than water based IPMCs. Operation of water based IPMCs at voltages above 1.23 volt is prohibitive due to concomitant electrolysis of water [Bar-Cohen (2004)]. Ionic liquid based IPMCs can operate at an input voltage as high as 7 volt and therefore produce large displacements [Shahinpoor et al. (1998)]. For the present study, IPMC flapping wing is assumed to be made of 1-ethyl-3-methylimidazolium trifluoromethanesulfonate (EMI-Tf) ionic liquid as a solvent and can be made by the manufacturing method proposed by Akle et al. (2006).

Extensive work has been done in modeling the sensing and actuation mechanisms of IPMCs. Current modeling work can be classified into three categories based on their complexity levels [Shahinpoor and Kim (2004)]. In the most complex form, white box or physical models attempt to explain the underlying physics for the sensing and actuation responses of IPMCs [Nemat-Nasser and Li (2000), Porfiri (2009)]. For these models, researchers model the underlying mechanism of the electro-mechanical response and subsequent deformation (actuation) or sensing (electrical output). These models can accurately predict the bending behavior of IPMCs, but they need many predetermined physical and chemical properties which are measured in experiments. As a result, white box or physical models may not be practical to use for engineering design and analysis. On the other hand, black

box models, also called empirical models and phenomenological models, are based on system identification and the physical features are only a minor consideration [Kanno et al. (1994), Xiao and Bhattacharya (2001)]. These models offer minimal insight into the governing mechanisms within the IPMCs. Therefore, black box models are only applicable to specific shapes and boundary conditions. As a trade off between these two approaches, the gray-box models are based on physical laws and parameters determined by experiments. Gray box models can be more conveniently used to predict the behaviors of IPMCs with general shapes and boundary conditions [Lee et al. (2005), Newbury and Leo (2002)]. Buechler and Leo (2007) presented an energy-based method for modeling IPMC structures at high frequency range (0.1-500 Hz) which includes the typical flapping frequency of the natural flyers. With the availability of such models, feasibility studies for an IPMC flapping wing design have become possible.

In addition to the structural modeling, aerodynamic modeling aspects are necessary to analyze the performance of IPMC flapping wing configurations. Aerodynamic models used for the flapping wing flight can be broadly classified into quasi-steady models and unsteady models. The quasi-steady models assume low flapping frequencies so that shed wake effects are negligible [Betteridge and Archer (1974)]. In the unsteady models, unsteady aerodynamic characteristics are accounted for by the unsteady wake effects [DeLaurier (1993)]. Selected researchers have used computational fluid dynamics (CFD) to simulate the flapping flight [La Mantia and Dabnichki (2008), Pereira et al. (2009)]. CFD methods provide a clear picture of the flow by solving the incompressible form of the Navier-Stokes equations. However, CFD simulations are computationally intensive. DeLaurier (1993) proposed an unsteady aerodynamic model based on modified strip theory. The aerodynamic model makes it possible to estimate the aerodynamic performances of harmonically flapping wings in the phase of preliminary design and development [Ke et al. (2008)]. Various aerodynamic effects can be considered in this model such as camber effect, partial leading edge suction effect, viscous effect, unsteady wake effect and dynamic stall model of pitching motion. Therefore, the DeLaurier model is useful for estimating the lift generated by a flapping wing.

In this paper, structural modeling of an IPMC flapping wing is done using variational principle. Dynamic characteristics of IPMC flapping wings, having the same size as to the actual wings of three different dragonfly species, are analyzed using numerical simulations. An unsteady aerodynamic model is used to obtain the aerodynamic forces. Finally, a comparative study of performances of three IPMC flapping wings is performed.

2 Structural Modeling

The schematic diagram of the IPMC flapping wing geometry used for the structural modeling is shown in Fig. 1. Cantilever configuration of IPMC flapping wing is the equivalent representation of the dragonfly wing as it is a thin and long structure attached to the body by thorax. The wing is initially straight and takes the deformed shape when a voltage is applied, as shown in Fig. 1. The flapping wing is fixed at the root and has a rectangular cross-section.

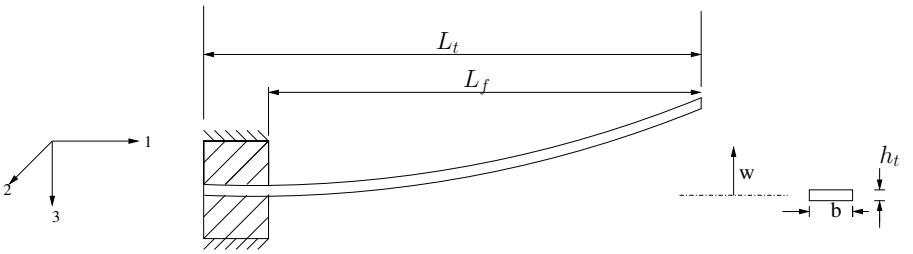

Figure 1: IPMC flapping wing geometry used for modeling.

An energy method is used to derive the equations of motion of the IPMC flapping wing [Buechler and Leo (2007)]. Kinetic energy of the IPMC flapping wing can be written as

$$T = \int_{V_{ol}} \frac{1}{2} \rho \dot{U}' \dot{U} dV_{ol} \tag{1}$$

where is the mechanical displacement. Since displacements are considered only in X_3 (flapping direction), mechanical displacement in this case can be represented as $w(x,t)$.

Potential energy of the IPMC wing can be expressed as

$$V = \int_{V_{ol}} \frac{1}{2} S' \mathbf{c^D} S - S' \mathbf{h} D + \frac{1}{2} D' \boldsymbol{\varepsilon}^{\mathbf{T^{-1}}} D \, dV_{ol} \tag{2}$$

Potential energy can be expressed in terms of displacements. Strain (S) is related to displacement vector through a differential operator L_u

$$S = L_u U \tag{3}$$

It can be seen from the Fig. 1 that the IPMC wing is slender and Euler-Bernoulli small deflection assumption is valid in this case. Therefore, the differential operator

(L_u) can be expressed as

$$L_u = -z\frac{\partial^2}{\partial X_1^2} \tag{4}$$

The strain distribution in the IPMC wing that is assumed to satisfy the Euler-Bernoulli assumption is

$$S_{11} = -z\frac{\partial^2 \mathrm{w(x,t)}}{\partial X_1^2} \tag{5}$$

The external work done, consisting of both mechanical and electrical work done, can be expressed as

$$W^{ext} = \int_{V_{ol}} fU + vD\,dV_{ol} \tag{6}$$

Here, v is the electrode potential applied on each electrode. In this present study, f and v are assumed to be harmonic forcing functions. Moreover, only one electrode on each side of the IPMC wing is assumed so $v(X) = v$.

The method of assumed mode shapes is used to express mechanical and electrical displacements as an infinite series

$$U(X,t) = \sum_{n=1}^{\infty} \Phi_{un}(X) A_n(t) \tag{7}$$

$$D(X) = \sum_{n=1}^{\infty} \Phi_{Dn}(X) q_n(t) \tag{8}$$

Here Φ_{un} and Φ_{Dn} are the mechanical and electrical mode shape functions, respectively. These shape functions must satisfy the kinematic boundary conditions. Mode shapes of an uncoupled beam are assumed to be good approximation for the mechanical shape functions in the present study and can be expressed as

$$\Phi_{un} = \cosh(\beta_n X_1) - \cos(\beta_n X_1) - \sigma_n[\sinh(\beta_n X_1) - \sin(\beta_n X_1)] \tag{9}$$

where

$$\beta_n^4 = \frac{\rho A \omega_n^2}{EI}$$

and

$$\sigma_n = \frac{\cosh(\beta_n L_f) + \cos(\beta_n L_f)}{\sinh(\beta_n L_f) + \sin(\beta_n L_f)} \tag{10}$$

Electric displacements are assumed to be constant and all charge is assumed to be present on the surface resulting in

$$\Phi_{D_{upper}} = \frac{1}{bL_t} \text{ and } \Phi_{D_{lower}} = \frac{-1}{bL_t} \tag{11}$$

In order to substitute the mechanical and electrical displacements in the energy expressions, the summations in Eqs. 7 and 8 are truncated to a finite sum and can be written in matrix form as

$$U(X,t) = \Phi'_u(X)A(t) \tag{12}$$

$$D(X) = \Phi_D(X)q(t) \tag{13}$$

Substituting the expression for in the kinetic energy yields

$$T = \int_{V_{ol}} \frac{1}{2}\rho \dot{A}' \Phi_u \Phi'_u \dot{A}\, dV_{ol} \tag{14}$$

Substituting the expressions for mechanical and electrical displacements in the potential energy yields

$$V = \int_{V_{ol}} \frac{1}{2} A' \left(L_u \Phi'_u\right)' \mathbf{c^D} \left(L_u \Phi_u\right) A - A' \left(L_u \Phi'_u\right)' \mathbf{h} \Phi'_D q + \frac{1}{2} q' \Phi_D \boldsymbol{\varepsilon}^{\mathbf{T}^{-1}} \Phi'_D q \, dV_{ol} \tag{15}$$

Similarly, external work done becomes

$$W^{ext} = \int_{V_{ol}} f \Phi'_u A + vq \, dV_{ol} \tag{16}$$

Governing equations are obtained using Hamilton's principle, which states that

$$\int_{t_1}^{t_2} \left(\delta T - \delta V + \delta W^{ext}\right) dt = 0 \quad \delta|_{t_1}^{t_2} = 0 \tag{17}$$

Here, δT is the variation in kinetic energy, δV is the variation in potential energy and δW^{ext} is the variation in work done by the external force. The variation in kinetic energy can be expressed as

$$\delta T = \int_{V_{ol}} \rho \, \delta A' \Phi_u \Phi'_u \dot{A} \, dV_{ol} \tag{18}$$

After integrating by parts and applying the condition stated in Eq. 17 that the variations are zero at t_1 and t_2, Eq. 18 becomes

$$\delta T = \delta A' \left(\int_{V_{ol}} -\rho \Phi_u \Phi_u' dV_{ol} \right) \ddot{A} \tag{19}$$

Similarly, the variation in strain energy is

$$\delta V_{se} = \delta A' \left[\int_{V_{ol}} \left(L_u \Phi_u' \right)' \mathrm{c}^{\mathrm{D}} (j\omega) \left(L_u \Phi_u' \right) dV_{ol} \right] A \tag{20}$$

The variation in coupling potential energy is

$$\delta V_{couple} = -\delta A' \left[\int_{V_{ol}} \left(L_u \Phi_u' \right)' \mathrm{h} (j\omega) \Phi_D' dV_{ol} \right] q - \delta q' \left[\int_{V_{ol}} \Phi_D \mathrm{h'} (j\omega) \left(L_u \Phi_u' \right) dV_{ol} \right] A \tag{21}$$

The variation in dielectric potential energy is

$$\delta V_{dielectric} = \delta q' \left[\int_{V_{ol}} \Phi_D \varepsilon^{\mathrm{T}^{-1}} (j\omega) \Phi_D' dV_{ol} \right] q \tag{22}$$

The variation in external work done is

$$\delta W^{ext} = \delta A' \Phi_u' f' + \delta q' \delta V' \tag{23}$$

Considering all the variations of the energy terms and applying Hamilton's principle, the resulting equation can be expressed as

$$\delta A' \left(-\mathbf{M_s} \ddot{A} - \mathbf{K_s}(j\omega) A - \Psi(j\omega) q + \Phi_u f' \right) + \delta q' \left(-\Psi'(j\omega) A - \mathbf{C^{-1}}(j\omega) q + V' \right) = 0 \tag{24}$$

where

$$\begin{aligned} \mathbf{M_s} (j\omega) &= \int_{V_{ol}} \rho \Phi_u \Phi_u' \dot{A} \, dV_{ol} \\ \mathbf{K_s} (j\omega) &= \int_{V_{ol}} \left(L_u \Phi_u' \right)' \mathrm{c}^{\mathrm{D}} (j\omega) \left(L_u \Phi_u' \right) dV_{ol} \\ \mathbf{\Psi} (j\omega) &= -\int_{V_{ol}} \left(L_u \Phi_u' \right)' \mathrm{h} (j\omega) \Phi_D' dV_{ol} \\ \mathbf{C^{-1}} &= \int_{V_{ol}} \Phi_D \varepsilon^{\mathrm{T}^{-1}} (j\omega) \Phi_D' dV_{ol} \end{aligned} \tag{25}$$

For arbitrary variations, the terms in the parenthesis of Eq. 24 must be equal to zero for the equality to be satisfied. The resulting equations in the frequency domain can be written in a matrix form

$$\begin{bmatrix} -\mathrm{M_s}\omega^2 + \mathrm{K_s}(j\omega) & \Psi(j\omega) \\ \Psi'(j\omega) & \mathrm{C}^{-1}(j\omega) \end{bmatrix} \begin{Bmatrix} A(j\omega) \\ q(j\omega) \end{Bmatrix} = \begin{Bmatrix} \Phi'_u f'(j\omega) \\ v'(j\omega) \end{Bmatrix} \tag{26}$$

Carrying out the integration in Eq. 25 yields diagonal mass ($\mathbf{M}_s$) and stiffness ($\mathbf{K}_s$) matrices because the mechanical shape functions in Eq. 9, are orthogonal to each other. Since the voltage is constant over the single electrode, the coupling vector (Ψ) is a column vector and the inverse of the capacitance (C^{-1}) is a scalar. Therefore, expressions of the above mentioned elements pertaining to the IPMC flapping wing structure, as shown in Fig. 1, are given as

$$C^{-1} = \frac{h_t}{\varepsilon_{33}^T b L_t}$$

$$M_{nn} = \rho b h_t L_f$$

$$K_{nn} = \frac{1}{12} c_{11}^D b h_t^3 L_f \beta_n^4$$

$$\Psi_{n1} = -h_{13} \frac{h_t^2}{2L_t} \int_0^{L_f} \Phi_{un,xx}(x)\, dx$$

Finally, matrices in Eq. 26 are evaluated for each frequency of interest and then solved for the generalized coordinates through matrix inversion

$$\begin{Bmatrix} A(j\omega) \\ q(j\omega) \end{Bmatrix} = \begin{bmatrix} -\mathbf{M_s}\omega^2 + \mathbf{K_s}(j\omega) & \Psi(j\omega) \\ \mathbf{\Psi'}(j\omega) & \mathbf{C^{-1}}(j\omega) \end{bmatrix}^{-1} \begin{Bmatrix} \Phi'_u f'(j\omega) \\ v'(j\omega) \end{Bmatrix} \tag{27}$$

In turn, deflection shape of the flapping wing can be determined due to a voltage input using Eq. 12.

3 Aerodynamic Modeling

The aerodynamic model is based on the modified strip theory as proposed by DeLaurier [DeLaurier (1993)], in which the aerodynamic forces of the flapping wing are obtained by integrating the sectional aerodynamic forces calculated in each section. The aerodynamic model is a well validated model and several researchers [Madangopal et al. (2005), Ke et al. (2008)] have used it in order to estimate the aerodynamic performance of harmonically flapping wings in the phase of preliminary design and development. In this unsteady aerodynamic model, the kinematics

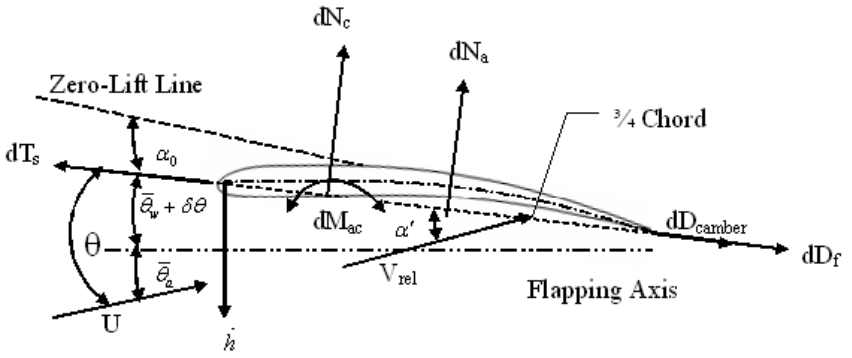

Figure 2: Aerodynamic forces and motion variables of a wing section.

for a section of the wing is represented by a plunging velocity $\dot{h}$ and a pitch angle of the chord $\dot{\theta}$ relative to the free stream velocity, as shown in Fig. 2.

The local parameters determining the forces includes the section's geometry, relative angle of attack at the $3/3$-chord location, pitch rates and the dynamic pressure at the $1/4$-chord location. The aerodynamic forces acting on each section of the wing are divided into the normal force dN, and the chordwise force, dF_X. The components of the normal force are: (i) dN_c, a circulatory force normal to the chord at the $1/4$-chord location and (ii) dN_a, an apparent-mass force normal to the chord at the $1/2$-chord location. The expressions for the normal force components are as follows:

$$dN_c = \frac{\rho_{air} UV}{2} C_n c dy \tag{28}$$

$$dN_a = \frac{\rho_{air} \pi c^2}{4} \dot{v}_2 dy \tag{29}$$

Therefore, the section's total attached flow normal force is

$$dN = dN_c + dN_a \tag{30}$$

The components of the chordwise force are: (i) dT_s, a chordwise leading edge suction force, (ii) dD_{camber}, a chordwise drag due to camber, and (iii) dD_f, a chordwise drag due to skin friction. The expressions for the chordwise force components are as follows:

$$dT_s = \eta_s 2\pi \left(\alpha' + \bar{\theta}_a - \frac{c\dot{\theta}}{4U} \right)^2 \frac{\rho_{air} UV}{2} c dy \tag{31}$$

$$dD_{camber} = -2\pi\alpha_0 \left(\alpha' + \bar{\theta}_a + \bar{\theta}_w\right) \frac{\rho_{air} UV}{2} cdy \tag{32}$$

$$dD_f = (C_d)_f \frac{\rho_{air} V_x^2}{2} cdy \tag{33}$$

Thus, the total chordwise force is

$$dF_X = dT_s - dD_{camber} - dD_f \tag{34}$$

The equations for the segment's instantaneous lift dL and thrust dT are

$$dL = dN\cos\theta + dF_X \sin\theta \tag{35}$$

$$dT = dF_X \cos\theta - dN\sin\theta \tag{36}$$

These may be integrated along the span to give the whole wing's instantaneous lift and thrust:

$$L(t) = 2\int_0^{\frac{b}{2}} \cos\gamma dL \tag{37}$$

$$T(t) = 2\int_0^{\frac{b}{2}} dT \tag{38}$$

where $\gamma(t)$ is the section's dihedral angle at that instant in the flapping cycle.

The wing's average lift and thrust are obtained by integrating $L(t)$ and $T(t)$ over the cycle. Integrating with respect to cycle angle, ϕ, instead of time, t, where

$$\phi = \omega t \tag{39}$$

so that the average lift and thrust are expressed as

$$\bar{L} = \frac{1}{2\pi}\int_0^{2\pi} L(\phi)d\phi \tag{40}$$

$$\bar{T} = \frac{1}{2\pi}\int_0^{2\pi} T(\phi)d\phi \tag{41}$$

4 Numerical Results

In order to validate the dynamic model, a numerical analysis is carried out for a cantilevered beam of dimensions 38 mm × 3 mm × 0.3 mm as used by Buechler and Leo (2007) in their experiment. Material properties of IPMCs exhibit strong

frequency dependence. Fig. 3 shows the frequency dependence of the strain coefficient which can be mathematically expressed as

$$d(s) = -216\frac{s+15}{(s+0.6)(s+14)(s+11000)}\frac{\mathrm{m}}{\mathrm{V}} \tag{42}$$

The magnitude of the strain coefficient decreases as frequency increases. The strain coefficient is related to the electro-mechanical coupling which produces deflections for an input voltage. The value of the strain coefficient is used to obtain free deflection at the tip. Fig. 4 shows the free deflection at the tip of the cantilevered beam and it matches well with the experimental result presented in Buechler and Leo (2007), thus verifying the implementation of IPMC model. Again, we see a reduction in the magnitude of the tip deflection with frequency. However, for this beam, there is a clear resonant peak at 16 Hz.

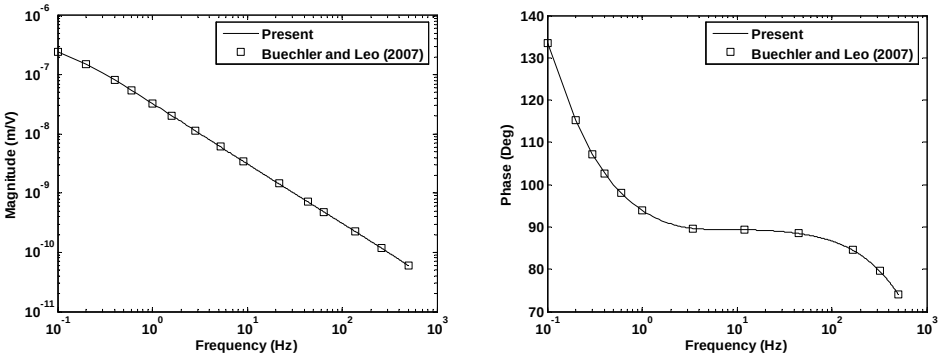

(a) (b)

Figure 3: Dependence of strain coefficient on frequency.

Insects, such as the dragonfly, fly with unusual aerial agility. Dragonfly flight satisfies all the requirements of an MAV flight envelope therefore providing inspiration for MAV design. Dragonfly wing size shows substantial variations among the different species due to demographical reasons. Fig. 5 shows the picture of three different dragonfly species and Table 1 shows the typical average values for their wings. Planforms of wings of three different dragonfly species are shown in Fig. 6. These three species provide wings with considerably different lengths and widths. Thus, they are different biomimetic designs for flapping wing MAVs.

IPMC wing corresponding to each dragonfly species is considered for dynamic analysis. Thickness and density of each IPMC flapping wing is selected as 0.3 mm and 2 g cm^{-3}, respectively [Shahinpoor et al. (1998)]. Therefore, mass of *Aeshna*

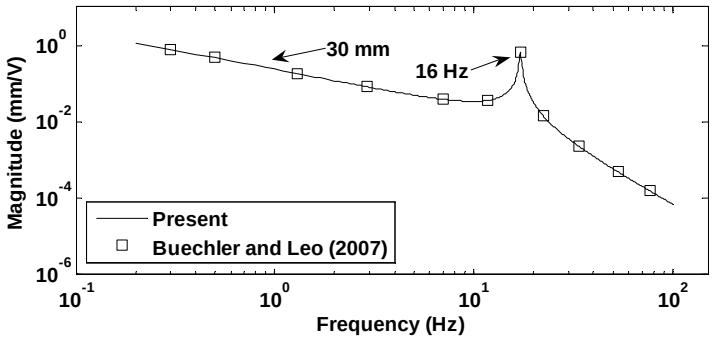

(a)

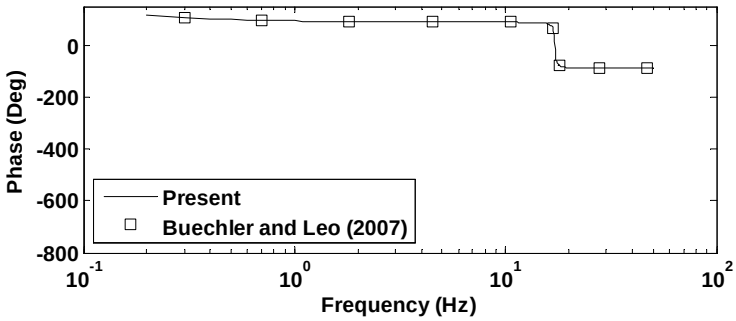

(b)

Figure 4: Free tip deflection at the tip of the cantilevered beam.

Table 1: Average values for wings of three different dragonfly species.

Species	**Length**	**Width**
Aeshna Multicolor[Combes and Daniel (2003)]	40 mm	10 mm
Anax Parthenope Julius [Sunada et al. (1998)]	53 mm	12 mm
Sympetrum Frequens [Azuma et al. (1985)]	67 mm	6.6 mm

Multicolor wing and *Anax Parthenope Julius* wing made of IPMC become 240 mg and 382 mg, respectively. Mass of the *Sympetrum Frequens* wing is obtained to be 265 mg.

Fig. 7 shows the first three mode shapes and corresponding natural frequencies of three dragonfly inspired IPMC flapping wings. Numerical results of the dynamic analysis of three different IPMC wings pertaining to the first mode shape are presented in this section because each flapping wing operates in its first mode.

(a) Dragonfly *Aeshna Multicolor*

(b) Dragonfly *Anax Parthenope Julius*

(c) Dragonfly *Sympetrum Frequens*

Figure 5: Picture of three different dragonfly species.

Fig. 8 shows the tip deflections of three different IPMC flapping wings at an excitation voltage of 1 V. It can be seen from the Fig. 8(a) that maximum tip deflection of *Aeshna Multicolor* wing is 1.12 mm and maximum tip deflection occurs at 21 Hz. Maximum tip deflection of *Anax Parthenope Julius* wing is 5.98 mm and maximum tip deflection occurs at 10.8 Hz as can be seen from Fig. 8(b). Similarly, Fig. 8(c) shows the maximum tip deflection of *Sympetrum Frequens* wing is 12.54 mm and it occurs at 8.4 Hz. Although input excitation voltage and thickness of each IPMC flapping wing is identical, magnitude of the maximum tip deflection and frequency at which it occurs are different. Therefore, the flapping frequency of each wing and the flapping angle produced by each wing will also be different. We will see in a later part of this section that these parameters have substantial effect on the performance of each wing in terms of aerodynamic forces.

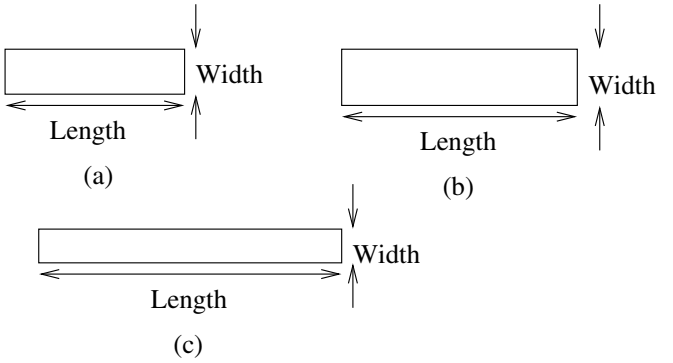

Figure 6: Schematic diagram of the planform of IPMC wings having the same size as (a) *Aeshna Multicolor* wing, (b) *Anax Parthenope Julius* wing and (c) *Sympetrum Frequens* wing.

Flapping angle can be obtained from the tip deflection following the procedure explained schematically in Fig. 9. Fig. 10 shows the flapping angle variations of IPMC flapping wings at an excitation voltage of 1 V. It can be seen from Fig. 10 that flapping angle of 2^0 is obtained for *Aeshna Multicolor* wing. Flapping angle reaches up to 8^0 for *Anax Parthenope Julius* wing and 12^0 for *Sympetrum Frequens* wing. This behavior can be attributed to the stiffness to mass ratio of each wing as evident from the fundamental frequencies in Fig. 7. The more flexible wings of *Sympetrum Frequens* are more suitable for high levels of flapping.

In order to analyze aerodynamic performances of these wings, aerodynamic forces are obtained using the unsteady aerodynamic model as described in the previous section.

For aerodynamic modeling, kinematics pertaining to the wing section located at 75% of the wing span is considered for calculation of the aerodynamic forces. Fig. 11 shows the average lift pertaining to each wing at different pitch angle ($\bar{\theta}_a$) at a flight speed of 3 m/s which is a typical flight speed for dragonflies. Average thrust at different pitch angles is shown in Fig. 12. It can be seen from Fig. 11 that maximum average lift for *Aeshna Multicolor* wing and *Anax Parthenope Julius* wing occur at the pitch angle of 7.5^0 and 7.6^0, respectively. Maximum average lift for *Sympetrum Frequens* wing occurs at the pitch angle of 7.7^0. However, it can be seen from Fig. 12 that thrust corresponding to each pitch angle, at which average lift reaches maximum, has a negative value. Since average thrust force must be positive to satisfy the condition for cruise flight, therefore the value of pitch angle is selected as 6.5^0 for each wing. From Figs. 11 and 12, it can be seen that the pitch

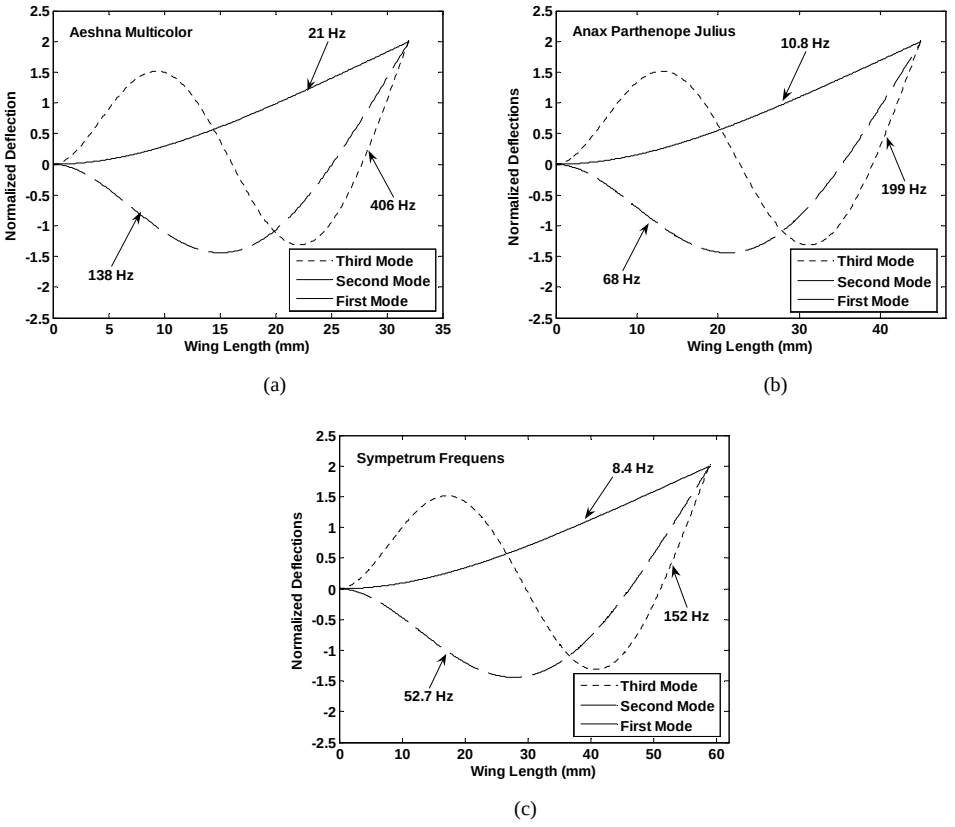

Figure 7: First three mode shapes and corresponding natural frequencies of three dragonfly inspired IPMC flapping wings.

angle of 6.5^0 results in a reasonable level of lift along with positive thrust.

Fig. 13 shows the average lift produced by smart flapping wings at different flight speeds. It can be seen from Fig. 13 that maximum lift force for *Aeshna Multicolor* IPMC wing is found to be 0.06 g which is less than its wing weight (0.24 g). Whereas, lift force for *Anax Parthenope Julius* IPMC wing and *Sympetrum Frequens* IPMC wing are 0.99 g and 1.16 g, respectively, which are more than their respective wing weight (0.382 g and 0.265 g, respectively). Average thrust force at different flight speeds is shown in Fig. 14. Average thrust force for *Aeshna Multicolor* wing is found to be 0.008 N at the flight speed of 7.1 m/s where lift force is maximum. Similarly, thrust force for *Anax Parthenope Julius* wing and *Sympetrum Frequens* wing are found to be 0.01 N and 0.007 N at the flight speed of 5.1 m/s and 4 m/s, respectively. The two flight speeds of 5.1 m/s and 4 m/s correspond to

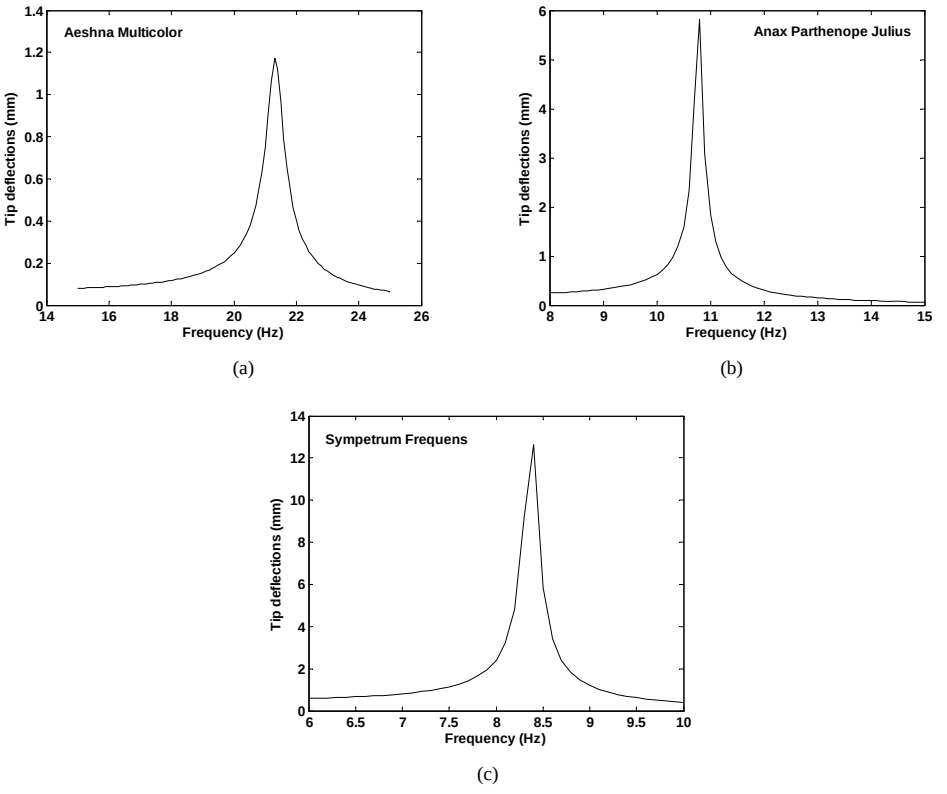

Figure 8: Tip deflections of three dragonfly inspired IPMC flapping wings.

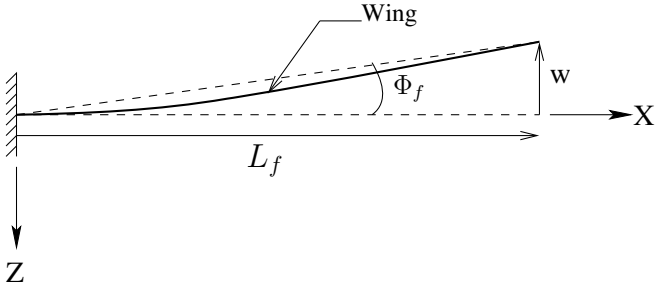

Figure 9: Schematic diagram of calculating flapping angle.

the maximum lift points in Figs. 13(b) and 13(c), respectively.

Fig. 15 shows the net lift force, obtained by subtracting the total wing weight from the total lift force, when two smart flapping wings are used for each species. Since

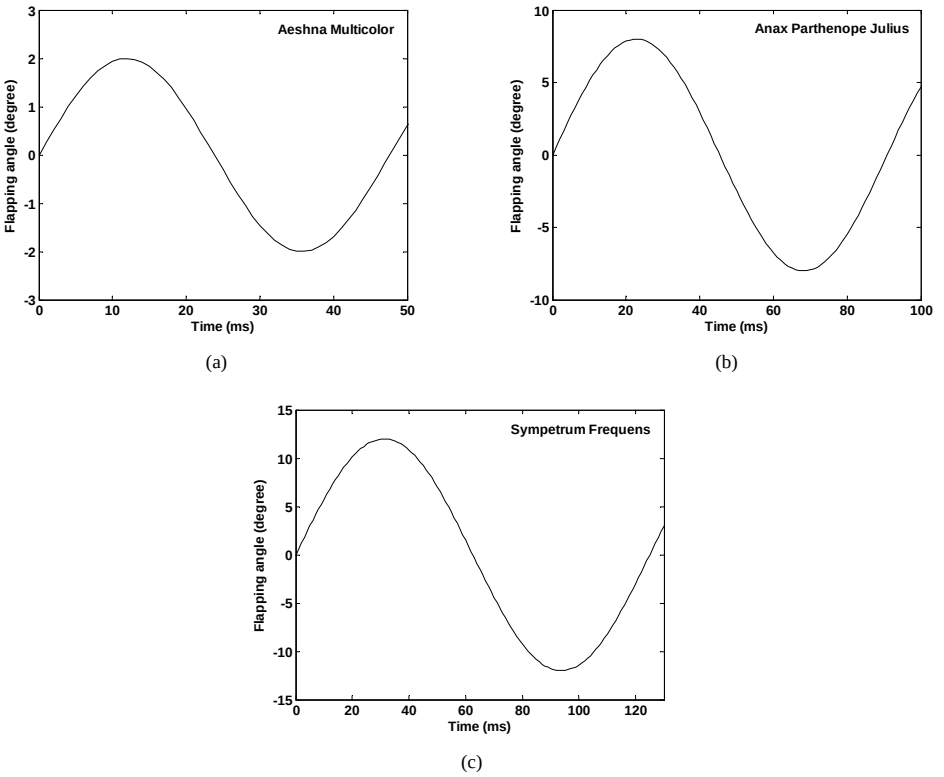

Figure 10: Flapping angle variations of three dragonfly inspired IPMC flapping wings.

lift force produced by each *Aeshna Multicolor* wing is less that its own weight at the excitation voltage of 1V, net lift is negative in this case. However, it can produce a positive net lift of 0.80 g when actuated at 5V and it occurs at the flight speed of 7.1 m/s as shown in Fig. 15(a). Fig. 15(b) shows the net lift force for the *Anax Parthenope Julius* wing is found to be 1.2 g at 1V and it occurs at the flight speed of 5.1 m/s. *Sympetrum Frequens* wing can produce a net lift force of 1.8 g at 1V and it occurs at the flight speed of 4 m/s as shown in Fig. 15(c). Net lift force produced by each IPMC flapping wing configuration may be used to carry payload in the form of power supply unit, control unit, sensory systems etc which are required for autonomous flight. From the numerical results in the paper, we see that biomimetic IPMC flapping wings based on the geometry of the dragonflies *Anax Parthenope Julius* wing and the *Sympetrum Frequens* wing represent attractive designs for insect scale flapping wing vehicles.

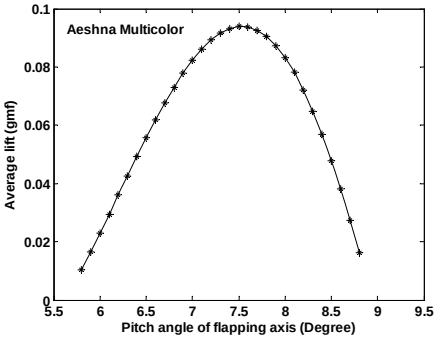

(a)

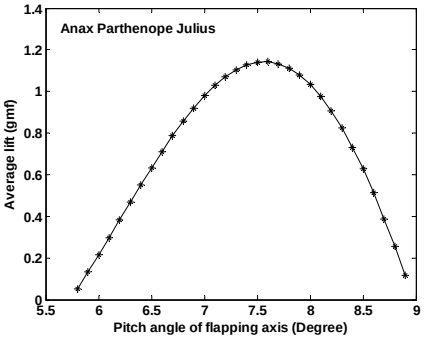

(b)

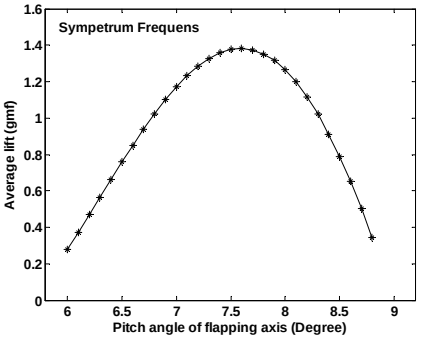

(c)

Figure 11: Average lift of three dragonfly inspired IPMC flapping wings for different pitch angle.

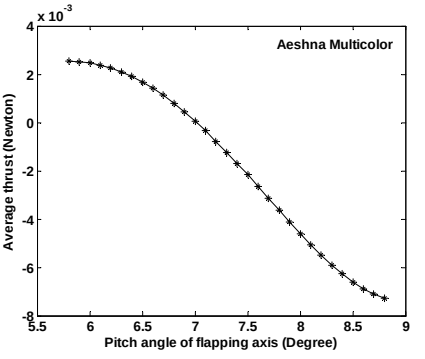

(a)

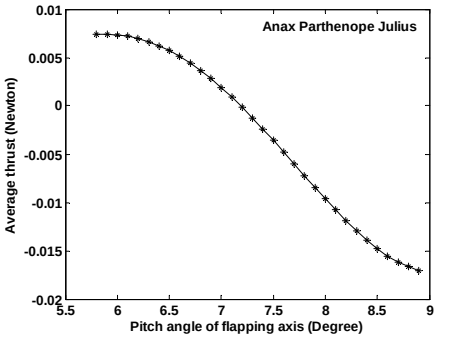

(b)

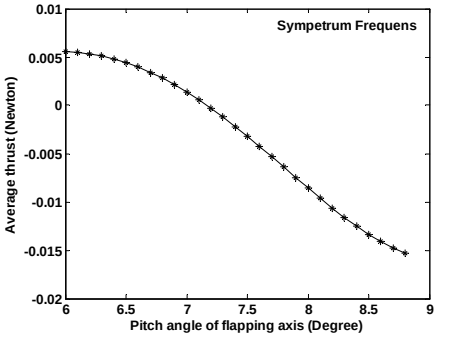

(c)

Figure 12: Average thrust of three dragonfly inspired IPMC flapping wings for different pitch angle.

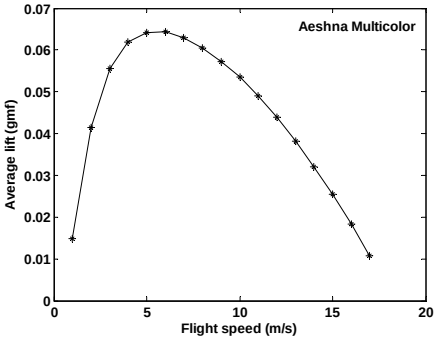

(a)

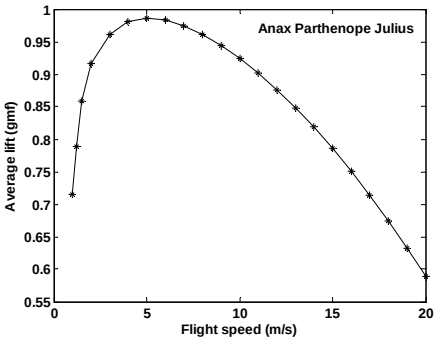

(b)

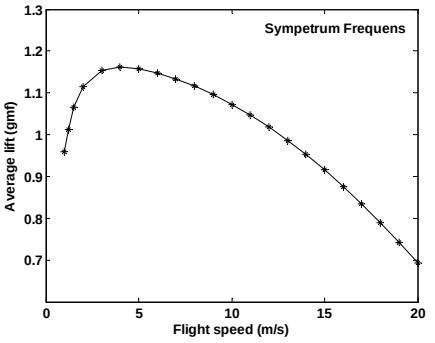

(c)

Figure 13: Average lift of three dragonfly inspired IPMC flapping wings for different flight speed.

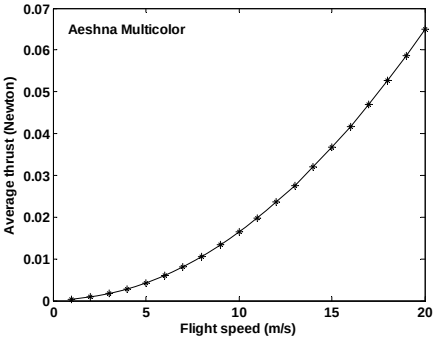

(a)

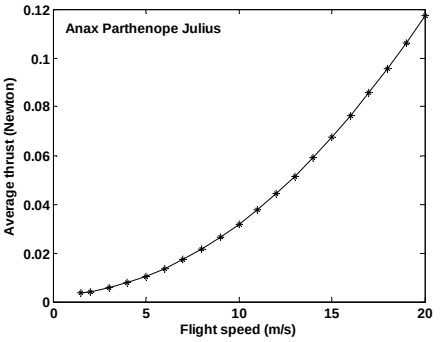

(b)

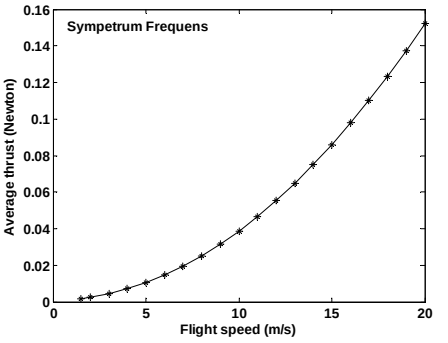

(c)

Figure 14: Average thrust of three dragonfly inspired IPMC flapping wings for different flight speed.

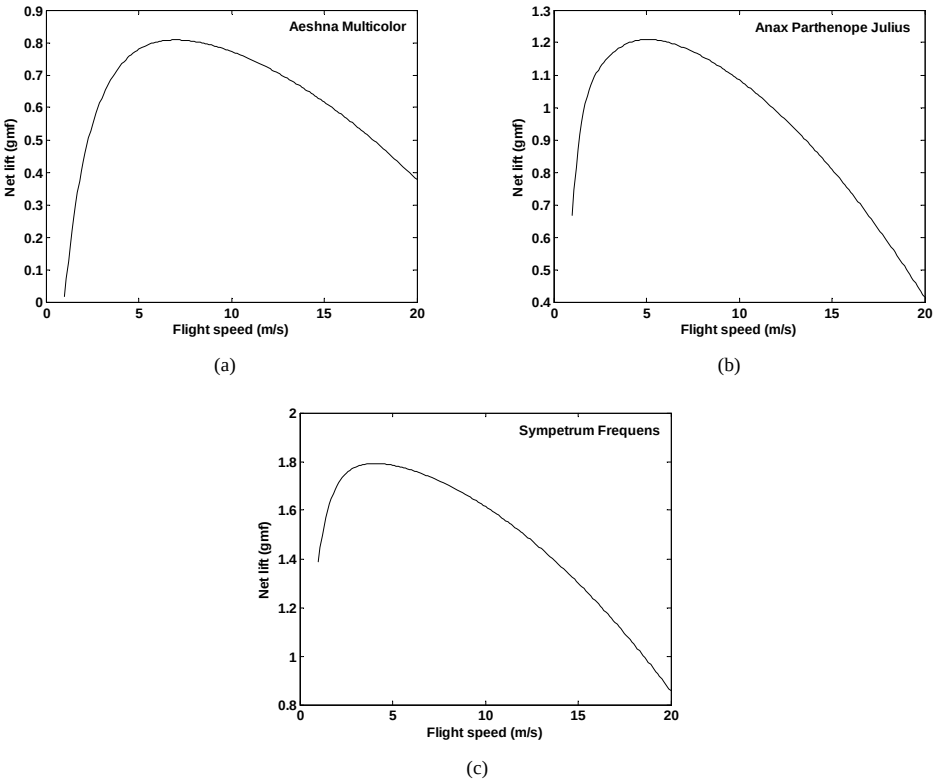

Figure 15: Net lift of three dragonfly inspired IPMC flapping wings for different flight speeds.

Before concluding this paper, we would like to make one point. This study is a computational search of dragonfly inspired IPMC flapping wings. This work paves the way for experimental studies on this topic.

5 Conclusions

In this study, variational principle is used for dynamic modeling of the IPMC flapping wing. Dynamic characteristics of IPMC flapping wings, having the same size corresponding to the actual wings of three different dragonfly species, are analyzed using numerical simulations. Dynamic characteristics of all the three different IPMC wings are studied for an input excitation voltage of 1V. An unsteady aerodynamic model is used to obtain the aerodynamic forces.

Flapping frequency of the IPMC flapping wing having the same size as *Aeshna*

Multicolor wing is 21 Hz which is highest among all the IPMC wings. However, it can produce a flapping angle of 2^0 which is lowest. It can be seen from its aerodynamic performance that it generates an average lift of 0.06 g which is less than its wing weight. Therefore, it can generate positive lift force at higher voltage, i.e., a positive lift of 0.80 g is obtained at 5V. Maximum lift force occurs at a flight speed of 7.1 m/s and thrust force at this flight condition is found to be 0.008 N at 1V. Although the wing can not generate positive net lift, it produces positive thrust force at 1V.

It can be see from the dynamic analysis of the IPMC flapping wing having the same size as *Anax Parthenope Julius* wing that it can produce a flapping angle of 8^0 at 10.8 Hz. Moreover, it can generate a lift force of 0.99 g at a flight speed of 5.1 m/s. Thrust force at the same flight condition is found to be 0.01 N which is highest among all the IPMC wings. A positive net lift force of 1.2 g is obtained for this wing.

A flapping angle of 12^0 is obtained for the IPMC wing having the same size as *Sympetrum Frequens* wing at 8.4 Hz. It can generate a lift force of 1.16 g which is highest among all the IPMC wings. Moreover, a positive net lift force of 1.8 g is obtained for this wing. Maximum lift force occurs at a flight speed of 4 m/s which shows that the wing is suitable for low speed flight. However, thrust force produced by the wing at the same flight condition is 0.007 N which is lowest.

The *Anax Parthenope Julius* and *Sympetrum Frequens* based IPMC flapping wing represent viable candidates for insect scale micro air vehicles.

References

Akle, B. J.; Bennett, M. D.; Leo, D. J. (2006): High-strain ionomeric ionic liquid electroactive actuators, *Sensors and Actuators A,* Vol. 126, pp. 173-181.

Ansari, S. A.; Zbikowski, R.; Knowles, K. (2006): Aerodynamic modelling of insect-like flapping flight for micro air vehicles, *Progress in Aerospace Sciences,* Vol. 42, pp. 129-172.

Apte, D. A.; Ganguli, R. (2009): Influence of temperature and high electric field on power consumption by piezoelectric actuated integrated structure, *CMC: Computers, Materials and Continua*, Vol. 10 (2), pp. 139-161.

Auricchio, F.; Petrini, L.; Pietrabissa, R.; Sacco, E. (2003): Numerical modeling of shape memory alloys in orthodontic, *CMES: Computer Modeling in Engineering and Sciences,* Vol. 4, pp. 365-380.

Azuma, A.; Azuma, S.; Watanabe, I.; Furuta, T. (1985): Flight mechanics of a dragonfly, *Journal of Experimental Biology*, Vol. 116, pp. 79-107.

Bar-Cohen, Y. (editor) (2004): *Electroactive Polymer (EAP) Actuators as Artificial Muscles - Reality, Potential, and Challenge*, SPIE, Washington.

Bennett, M. D.; Leo, D. J.; Wilkes, G. L.; Beyer, F. L.; Pechar, T. W. (2006): A model of charge transport and electromechanical transduction in ionic liquid-swollen nafion membranes, *Polymer,* Vol. 47, pp. 6782-6796.

Betteridge, D. S.; Archer, R. D. (1974): A study of the mechanics of flapping wings, *Aeronautical Quarterly*, Vol. 25, pp. 129-142.

Buechler, M. A.; Leo, D. J. (2007): Characterization and variational modeling of ionic polymer transducers, *Journal of Vibration and Acoustics,* Vol. 129 (1), pp. 113-120.

Cheng, C. H.; Chen, S. C. (2004): The Simulation of Diaphragm Deflection Actuated by Shear Mode Piezoelectric Actuator in Microdroplet Ejector, *CMC: Computers, Materials and Continua*, Vol. 1 (3), pp. 205-212.

Combes, S. A.; Daniel, T. L. (2003): Flexural stiffness in insect wings II. Spatial distribution and dynamic wing bending, *Journal of Experimental Biology*, Vol. 206 (17), pp. 2989-2997.

Cox, A.; Monopoli, D.; Cveticanin, D.; Goldfarb, M.; Garcia, E. (2002): The development of elastodynamic components for piezoelectrically actuated flapping micro-air vehicles, *Journal of Intelligent Material Systems and Structures*, Vol. 13 (9), pp. 611-615.

DeLaurier, J. D. (1993): An aerodynamic model for flapping-wing flight. *Aeronautical Journal*, Vol. 97 (964), pp. 125-130.

Dickinson, M. H.; Lehmann, F. O.; Sane, S. P. (1999): Wing rotation and the aerodynamic basis of insect flight, *Science*, Vol. 284 (5422), pp. 1954-1960.

Ganguli, R.; Gorb, S.; Lehmann, F. O.; Mukherjee, S.; Mukherjee, S. (2010): An experimental and numerical study of C*alliphora* wing structure, *Experimental Mechanics,* Vol. 50 (8), pp. 1183-1197

Ghosh, D. P.; Gopalakrishnan, S. (2004): Role of coupling terms in constitutive relationships of magnetostrictive materials, *CMC: Computers, Materials and Continua*, Vol. 1 (3), pp. 213-228.

Kanca, E; Eskil, M. (2009): Comparison of new formulations for martensite start temperature of Fe-Mn-Si shape memory alloys using genetic programming and neural networks, *CMC: Computers, Materials and Continua*, Vol. 10 (1), pp. 65-95.

Kanno, R.; Kurata, A.; Hattori, M.; Tadokoro, S.; Takamori, T.; Oguro, K. (1994): Characteristics and modeling of ICPF actuators *Proc. Japan–USA Symposium on Flexible Automation*, Vol. 2, pp 691–698

Ke, S.; Zhigang, W.; Chao, Y. (2008): Analysis and flexible structural modeling for oscillating wing utilizing aeroelasticity, *Chinese Journal of Aeronautics*, Vol. 21 (5), pp. 402-410.

Kesel, A. B.; Philippi, U.; Nachtigall, W. (1998): Biomechanical aspects of the insect wing: an analysis using the finite element method, *Computers in Biology and Medicine*, Vol. 28 (4), pp. 423-437.

La Mantia, M.; Dabnichki, P. (2008): Unsteady 3D boundary element method for oscillating wing, *CMES: Computer Modeling in Engineering and Sciences,* Vol. 33 (2), pp. 131-153.

Lee, S.; Park, H. C.; Kim, K. J. (2005): Equivalent modeling for ionic polymer-metal composite actuators based on beam theories, *Smart Materials & Structures*, Vol. 14 (6), pp. 1363-1368.

Lee, S. G.; Park, H. C.; Pandita, S. D.; Yoo, Y. (2006): Performence improvement of IPMC (Ionoc Polymer Metal Composite) for a flapping actuator, *International Journal of Control, Automation, and Systems,* Vol. 4 (6), pp. 748-755.

Madangopal, R.; Khan, Z. A.; Agrawal, S. K. (2005): Biologically inspired design of small flapping wing air vehicles using four-bar mechanisms and quasi-steady aerodynamics, *Journal of Mechanical Design*, Vol. 127 (4), pp. 809-816.

McIntosh, S. H.; Agrawal, S. K.; Khan, Z. (2006) Design of a mechanism for bi-axial rotation of a wing for a hovering vehicle, *IEEE/ASME Transaction on Mechatronics*, Vol. 11 (2), pp. 145-153.

Nemat-Nasser, S.; Li, J. Y. (2000): Electromechanical response of ionic polymer-metal composites, *Journal of Applied Physics*, Vol. 87 (1), pp. 3321–3331.

Newbury, K. M.; Leo, D. J. (2002): Electromechanical modeling and characterization of ionic polymer benders, *Journal of Intelligent Material Systems and Structures*, Vol. 13 (1), pp. 51–60.

Park, H. C.; Lee, S.; Kim, K. J. (2005): Equivalent modeling for shape design of IPMC (Ionic Polymer Metal Composite) as flapping actuator, *Key Engineering Materials,* Vol. 297-300, pp. 616-621.

Pereira, J. M. C.; Maia, N. A. R.; Pereira, J. C. F. (2009): A computational fluid dynamics study of a 2D airfoil in hovering flight under ground effect, *CMES: Computer Modeling in Engineering and Sciences,* Vol. 49 (2), pp. 113-141.

Porfiri, M. (2009): An electromechanical model for sensing and actuation of ionic polymer metal composites, *Smart Materials & Structures*, Vol. 18 (1), pp. 015016 (16pp).

Raney, D. L.; Slominski, E. C. (2004): Mechanization and control concepts for biologically inspired micro aerial vehicles, *Journal of Aircraft*, Vol. 41 (6), pp.

1257-1265.

Sladek, J.; Sladek, V.; Zhang, C.; Sanche, F. G.; Wunsche, M. (2006): Meshless local Petrov-Galerkin method for plane piezoelectricity. *CMC: Computers, Materials and Continua*, Vol. 4 (2), pp. 109-118.

Shahinpoor, M.; Bar-Cohen, Y.; Simpson, J. O.; Smith, J. (1998): Ionic polymer-metal composites (IPMCs) as biomimetic sensors, actuators and artificial muscles - A review, *Smart Materials & Structures*, Vol. 7 (6), pp. R15-R30.

Shahinpoor, M.; Kim, K.J. (2004): Ionic polymer-metal composites: III. Modeling and simulation as biomimetic sensors, actuators, transducers, and artificial muscles, *Smart Materials & Structures*, Vol. 13 (6), pp. 1362-1388.

Singh, B.; Chopra, I. (2008): Insect-based hover-capable flapping wings for micro air vehicles: Experiments and analysis, *AIAA Journal*, Vol. 46 (9), pp. 2115-2135.

Sunada, S.; Zeng, L. J.; Kawachi, K. (1998): The relationship between dragonfly wing structure and torsional deformation, *Journal of Theoretical Biology*, Vol. 193 (1), pp. 39-45.

VandenBerg, C.; Ellington C. P. (1997): The vortex wake of a 'hovering' model hawkmoth, *Philosophical Transactions of the Royal Society of London Series B-Biological Sciences*, Vol. 352 (1351), pp. 317-328.

Wang, H.; Zeng, L. J.; Yin, C. Y. (2002): Measuring the body position, attitude and wing deformation of a free flight dragonfly by combining a comb fringe pattern with sign points on the wing, *Measurement Science & Technology*, Vol. 13 (6), pp. 903-908.

Wu, C. P.; Lo, J. Y.; Chao, J. K. (2005): A three-dimensional asymptotic theory of laminated piezoelectric shells, *CMC: Computers, Materials and Continua*, Vol. 2 (1), pp. 119-138.

Xiao, Y; Bhattacharya, K. (2001): Modeling electromechanical properties of ionic polymers, *Proc. SPIE*, Vol. 4329, pp. 292-300.

Yamada, T.; Yoshimura, S. (2008): Line search partitioned approach for fluid-structure interaction analysis of flapping wing, *CMES: Computer Modeling in Engineering and Sciences,* Vol. 24 (1), pp. 51-60.

Yamamoto, M.; Isogai, K. (2005): Measurement of unsteady fluid dynamics forces for a mechanical dragonfly model, *AIAA Journal*, Vol. 43 (12), pp. 2475-2480.

Zhang, J.; Lu, X. Y. (2009): Aerodynamic performance due to forewing and hindwing interaction in gliding dragonfly flight, *Physical Review E*, Vol. 80 (1), pp. 017302-4.

Zhang, T. Y. (2004): Dielectric breakdown model for an electrically impermeable

crack in a piezoelectric material, *CMC: Computers, Materials and Continua*, Vol. 1 (1), pp. 107-116.

Zhou, H; Zhou, Y.; Zheng, X. (2007): Numerical Simulation of Nonlinear Dynamic Responses of Beams Laminated with Giant Magnetostrictive Actuators, *CMC: Computers, Materials and Continua*, Vol. 6 (3), pp. 201-212.